Journal of Hydrology: Regional Studies 60 (2025) 102462

Contents lists available at ScienceDirect

Journal of Hydrology: Regional Studies

journal homepage: www.elsevier.com/locate/ejrh

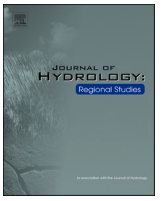

Spatial variability of hydraulic conductivity of the Cretaceous aquifer in Belgium

Miguel Moreno Gómez [a,*], Gert Ghysels [b], Syed M.T. Mustafa [c], Simon Six [d], Alexander Vandenbohede [d], Tom Diez [d], Dirk Gijsbert Cirkel [e], Marijke Huysmans [a]

[a] Department of Water and Climate, Vrije Universiteit Brussel, Pleinlaan 2, Brussels 1050, Belgium
[b] AGT Advanced Groundwater Techniques, Kontich 2550, Belgium
[c] Hydrology and Environmental Hydraulics Group, Wageningen University, Wageningen, AA 6700, the Netherlands
[d] De Watergroep, Vooruitgangstraat 189, Brussel 1030, Belgium
[e] KWR Water Research Institute, Nieuwegein, PE 3433, the Netherlands

ARTICLE INFO

Keywords:
Hydraulic conductivity
Cretaceous aquifer
Chalk
Flanders
Belgium

ABSTRACT

Study region: Flanders (Belgium).
Study focus: The Cretaceous aquifer—consisting of chalk sediments and other forms of carbonates—is an important source of fresh water for drinking water and industry in Flanders. Therefore, maintaining optimal water quality and quantity in this aquifer is critical. However, uncertainty of the Cretaceous hydrogeological parameters is high due to its depth, confinement, scarce observation wells, and the complex lithostratigraphic formations and members, resulting in limited information on the aquifer hydrogeological properties.
New hydrogeological insights from the region: This work provides novel insights on the Cretaceous characterization, focused on the spatial distribution of hydraulic conductivity estimated through multiple pumping tests, geophysics, and flowmeter logs. A correlation between hydraulic conductivity and depth displays decreasing values as depth increases towards northern regions. The analysis indicates that the high heterogeneity of the Cretaceous and the spatial variability of hydraulic conductivity is led by lithological differences, including the presence of a hardground layer with variable thickness and permeability. This correlation also highlights the influence of fractures and karstification, enhancing hydraulic conductivity at shallower regions while decreasing it at deeper sections of the aquifer given the lower fracture density due to higher overburden pressures. Results demonstrate the influence of depth, lithology, and fracture development controlling the hydraulic conductivity variability within the Cretaceous, providing important insights for further research on water extraction and aquifer storage capacity, among others.

1. Introduction

In North-western Europe, Cretaceous chalk formations are crucial groundwater reservoirs. These chalk aquifers supply substantial volumes of water in countries such as Denmark, England, France, the Netherlands, and southern Sweden (Nygaard, 1993; Mendizabal and Stuyfzand, 2009; Maréchal and Rouillard, 2020). However, many of these aquifers have been categorized as "poor" according to

* Corresponding author.
E-mail address: miguel.moreno@vub.be (M. Moreno Gómez).

https://doi.org/10.1016/j.ejrh.2025.102462
Received 5 February 2025; Received in revised form 6 May 2025; Accepted 7 May 2025
Available online 15 May 2025

either quantitative and/or qualitative status as defined by the European Water Framework Directive (West et al., 2023). Additionally, climate change and extreme events such as droughts are expected to drive increased water demands in North-western Europe, putting additional pressure on chalk aquifers to fulfil regional water supply (Riediger et al., 2014). In Europe, the occurrence of longer periods of drought in recent years (2017, 2018, 2019, and 2020) have highlighted the negative impacts of these extreme events on groundwater, economy, and society (Rakovec et al., 2022). Therefore, preventing overexploitation and degradation of chalks aquifers in this European region is critical (Fig. 1).

Cretaceous aquifers in Belgium are formed by chalk deposits and other types of carbonates such as Marls and Calcarenites from the Late Cretaceous and Early Paleocene. Dependency on these aquifers is considerable since they supply approximately 20–25 % of the extracted water in the Walloon region at the southern part of the country (Goderniaux et al., 2023). In the Flemish-Brabant and Limburg, provinces in the northern region of Flanders, groundwater is the sole source of drinking water due to the existence of highly permeable porous and karstic aquifers; in these provinces, the Cretaceous aquifer provides more than 20 million m^3 per year for drinking water production (Ghysels and Mustafa, 2021). In the adjacent area of Dutch Limburg, a similar volume of drinking water is produced from the Cretaceous. In Flanders, the Cretaceous—or Krijt—is currently in a favourable quantitative and qualitative state, both for the phreatic and confined part of the aquifer, as defined in the European Water Framework Directive (2000/60/EG) and the Groundwater directive (2006/118/EG). However, monitoring in some areas is suggested and strategies to maintain this aquifer optimal, in terms of quantity and quality, are encouraged to face future water demand scenarios.

According to management reports of the Scheldt and Meuse river basins (Coordinated Commission for Integrated Water Policy -CIW- 2016), approximately 75 % of the permitted extraction rate in the Cretaceous aquifer is granted to the production of drinking water; the remaining 25 % of the permitted extraction volume is designated to supply water for industry, agriculture, energy production processes, and other services such as trade and transport. Therefore, the Cretaceous aquifer is of great importance from a societal and economic point of view, mainly in its confined part, because it is well protected against potential negative influences on the quality of the water. Given its importance, strategies to maintain optimal conditions for this aquifer, in terms of water quality and quantity, are a priority in the region of Flanders.

Aquifer characterization is a very important step to understand regional groundwater flows and the capacity of aquifer systems. Nevertheless, aquifer heterogeneity and the commonly sparse data of the subsurface complicate the three-dimensional characterization of aquifers' physical (e.g., porosity, permeability) and hydraulic properties (e.g., hydraulic conductivity, transmissivity). Among these properties, hydraulic conductivity is a critical parameter for groundwater research, including numerical modelling to determine scenarios of extraction, infiltration, storage, flow, and solute transport. Unfortunately, due to limitations for exploration and

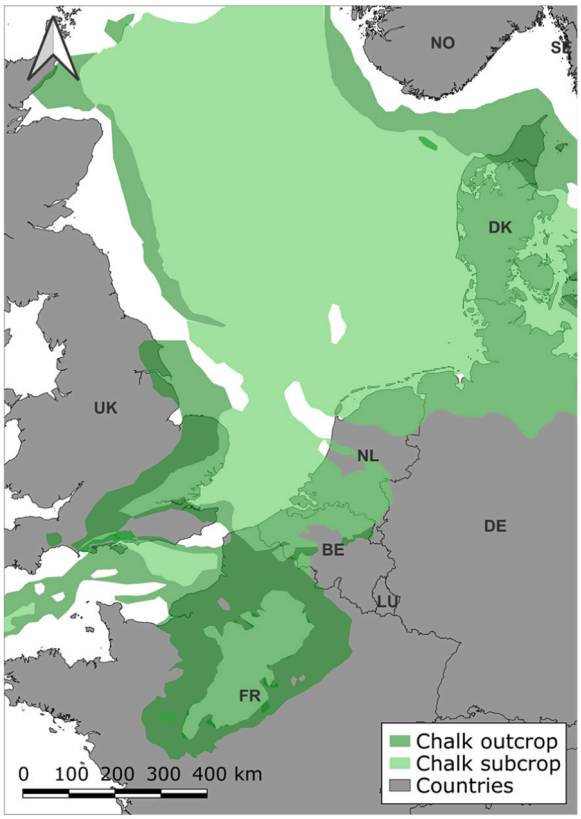

Fig. 1. Approximate distribution of chalk sediments in northern Europe. Digitalized after West et al. (2023).

the complexity of the subsurface, the spatial distribution of hydraulic conductivity—or other physical and/or hydraulic properties—is often poorly characterized or estimated through statistical methods (Dagan, 2002). For complex aquifer systems, an incomplete characterization applied to numerical models, could lead into erroneous predictions regarding to flow in terms of velocity and direction (Huysmans and Dassargues, 2009; Mustafa et al., 2020).

For hard rock systems, characterization of hydraulic conductivity is even more complicated due the different, and sometimes highly contrasting lithologies, the occurrence of hardgrounds, heterogeneous fracturing patterns, and the lack of data at deeper locations. In carbonate-type formations, such as chalks, estimating hydrogeological properties becomes even more challenging due to the dual porosity of such systems (Kovács, 2021; Worthington, 2023; Pappalardo et al., 2024; Xanke et al., 2024). The chemical composition of these formations, primarily formed by calcium carbonate ($CaCO_3$), makes this type of aquifers prone to dissolution if certain boundary conditions are fulfilled (Bauer et al., 2003; Liedl et al., 2003; Gillon et al., 2012). Therefore, in carbonate-type aquifers, hydraulic conductivity can vary by orders of magnitude, even at local scale, due to the hydraulic differences between the matrix continuum and intersected discrete fissures (Nativ et al., 2003). These characteristics are of the uttermost importance to be considered as part of conceptual and numerical models (Kordilla et al., 2012; Hartmann et al., 2014; West et al., 2023).

This paper aims to contribute to the understanding of the hydrogeology and spatial distribution of hydraulic conductivity of the Cretaceous aquifer in Flanders. Therefore, the objectives of this work are: **i)** analyse the heterogeneity of lithological formations within the Cretaceous, **ii)** integrate data from pumping tests, geophysics, and flowmeter logs to characterize spatial heterogeneity of hydraulic conductivity, and **iii)** identify predictor variables and models to describe the spatial distribution of hydraulic conductivity within the Cretaceous.

2. Study area

2.1. Flanders

Located in the northern part of Belgium, the region of Flanders comprises five provinces: Antwerp, East Flanders, Flemish Brabant, Limburg, and West Flanders (Fig. 2). Brussels is not part of Flanders but is a separate region. According to the Belgian statistical office, the population of Flanders reached 6774,807 inhabitants in 2023 (Belgian Federal Government, 2024). In Flanders, elevation ranges from −12–288 m relative to the Second General Levelling (m TAW)—the Belgium's official vertical reference system—as displayed by a Digital Terrain Model (National Geographic Institute, 2022). Given the topographic characteristics, Flanders contains coastal areas, lowlands, and elevated regions within its 13,626 km^2, holding a population density of approximately 497 inhabitants per km^2.

Given its proximity to the North Sea in the northwest, Flanders experiences a temperate maritime climate with annual precipitation average ranging between 675 and 995 mm (Batelaan et al., 2007; Zomlot et al., 2015; Speijer et al., 2024). The region's hydrology is dominated by an extensive network of surface water bodies, including rivers, channels, and lakes, which are crucial sources of water for agriculture, industry, and drinking water supply. An estimated volume of 345 million m^3 of drinking water is produced annually for a consumption per capita of about 84.8 l day^{-1} (Flemish Environment Agency, 2023). From this volume of produced drinking water, surface water accounts for approximately 53.7 %, while 46.3 % is extracted from aquifers (Flemish Environment Agency, 2023). In the Flemish-Brabant and Limburg provinces, groundwater is the sole source of drinking water due to the presence of highly permeable Neogene and Quaternary aquifers suitable for water production. These phreatic porous aquifers in this region have been the subject of important studies focused on modelling (Zwertvaegher et al., 2013; Vansteenkiste et al., 2016; Casillas-Trasvina et al., 2022), water quality (Coetsiers et al., 2009; Possemiers et al., 2014; Van Camp et al., 2017), and hydraulic conductivity and permeability (Huysmans et al., 2008; Possemiers et al., 2012; Rogiers et al., 2012, 2013; Vandersteen et al., 2014) to name a few.

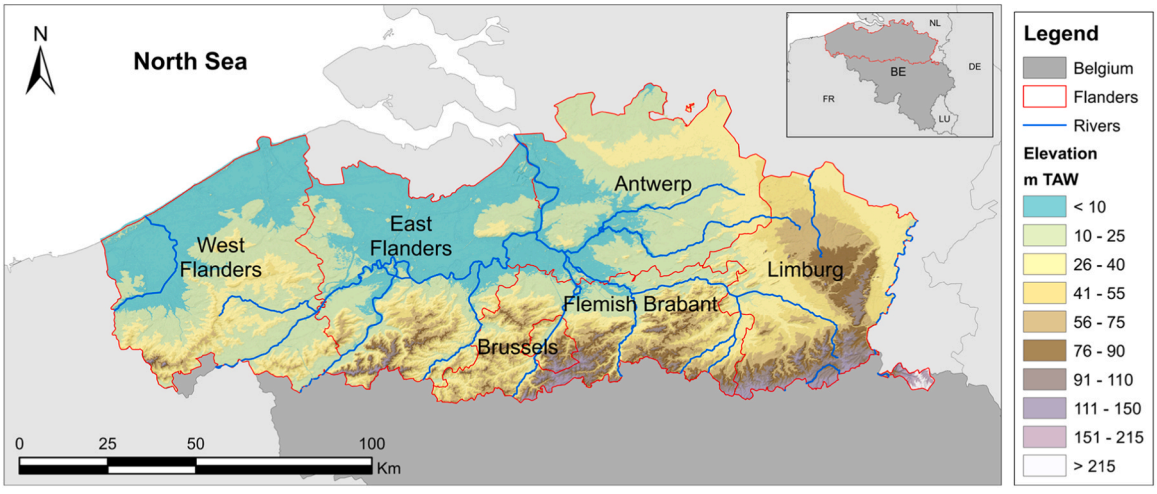

Fig. 2. Flanders division and elevation map.

In addition to the Neogene and Quaternary aquifers in Flanders, carbonate formations from the Late Cretaceous and Early Paleocene are a crucial source of drinking water. This Cretaceous aquifer is known for its high heterogeneity both horizontally and vertically. The mapping of its hydrogeological properties is a challenging task given the primary and secondary porosities, and the variability among its different lithological formations.

2.2. Cretaceous deposits in Flanders

The different formations and members that constitute the subsurface of Flanders are described according to the 3D geological model (G3Dv3) and a new 3D hydrogeological model (Databank Ondergrond Vlaanderen, 2019). The main units on which the model is discretized are grouped by age as: Quaternary, Neogene, Oligocene, Eocene, Paleocene, Cretaceous, Jurassic to Permian, Carboniferous, Devonian, and Silurian to Cambrian. As part of the model, the three-dimensional extension of carbonate-based formations are described based on multiple data obtained from drilling reports, measurements in boreholes, seismic information, and literature. Descriptions presented here are a revised update of the G3Dv2 model (Matthijs and Lagrou, 2007, 2010), and the reports presented by Deckers et al. (2019) and Ghysels and Mustafa (2021).

For consistency, the term 'Cretaceous' will hereinafter refer to the aquifer, encompassing carbonate formations from the Late Cretaceous as well as carbonate formations from the Early Paleocene. The Cretaceous formations are present on top of Palaeozoic deposits ranging in age from Cambrian to Carbonian (Lagrou and Dreesen, 2005). During the Late Cretaceous (Cenomanian to Maastrichtian), and Early Paleocene (Danian), carbonate deposition occurred in Flanders due to marine transgression and the tectonic inversion of the Jura basins; these events resulted in considerable lithological variability in the area (LeGrand, 1968). Cretaceous deposits extend over 91 % of Flanders, only missing along some topographical heights at the south of the Brabant Massif (Dusar and Lagrou, 2007). The thickness of the Cretaceous is variable, ranging from metres at the south, increasing northward; the thickest section

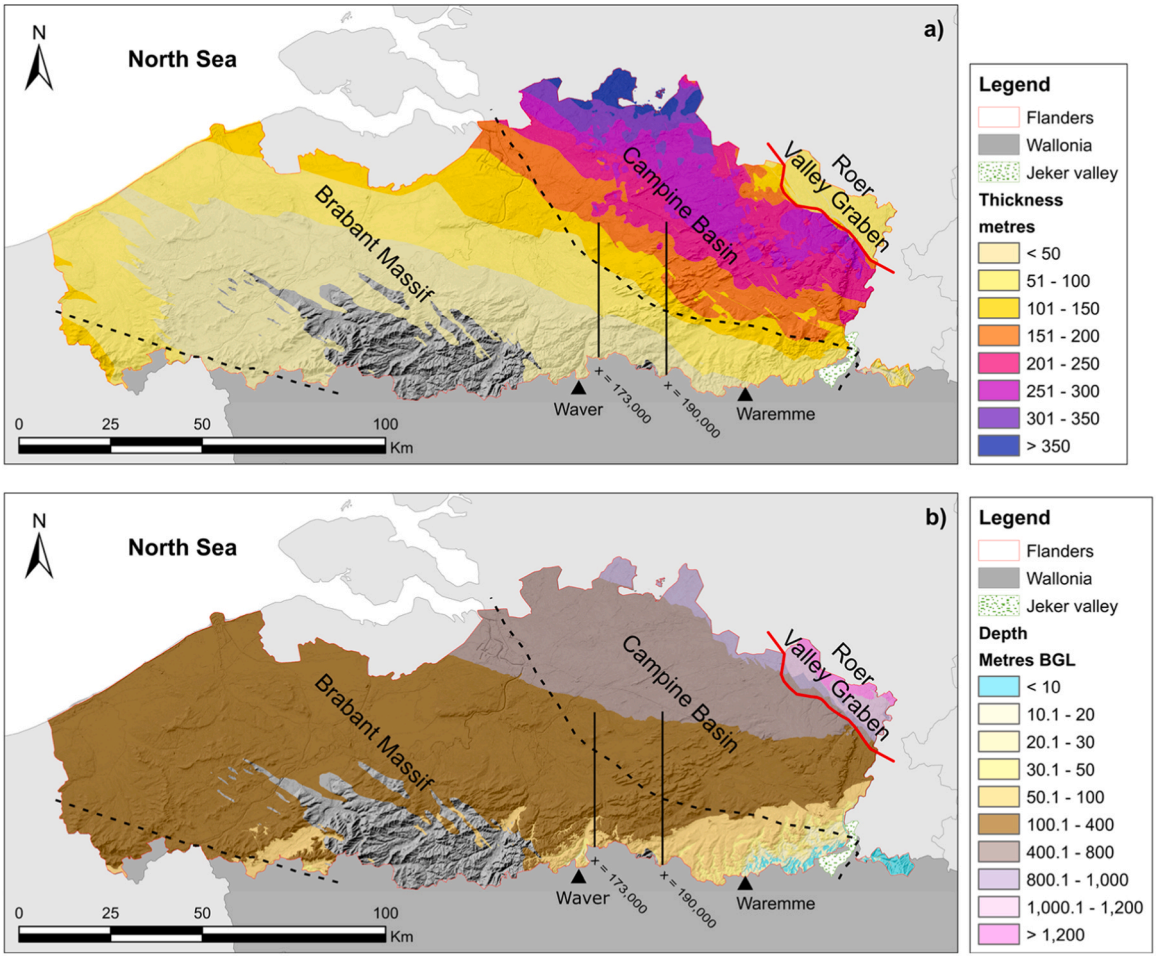

Fig. 3. The Cretaceous in Flanders. In a), the thickness of the Cretaceous; in b), the depth (top) of the Cretaceous in metres below ground level (BGL). Dotted lines indicate boundaries of the Brabant Massif. Red bolt line indicates the edge of the Roer Valley Graben. Continuous black lines indicate the geology cross sections displayed in Fig. 4.

of the Cretaceous is found in the Campine basin where its vertical extension reaches more than 300 m (Fig. 3a).

Although some outcrops occur in the southeast of Flanders, following the axis Waver, Waremme and the Jeker valley in the northern parts of Wallonia—the area in where the aquifer is primarily recharged by precipitation—the Cretaceous in Flanders is mostly covered by Tertiary and Quaternary deposits, and is therefore confined (Dassargues and Monjoie, 1993). The main confined units overlying the Cretaceous are the Ieperian, Bartoon, and Boom aquitards (Ghysels and Mustafa, 2021). From the outcrops in the southeast, located approximately at 200 m above sea level, the Cretaceous dips northward, with its top reaching approximately 800 m below sea level (Deckers et al., 2019). Similarly, deposits covering the Cretaceous exhibit a thickening pattern towards the north, ranging from metres in the southern areas to more than 1000 m in the Roer Valley Graben (Fig. 3b). Therefore, the subsurface of the region is composed by multiple layers forming phreatic aquifers, confining units, and confined aquifers. Examples of the complex lithology of the Flanders subsurface are displayed by cross-sections in Fig. 4.

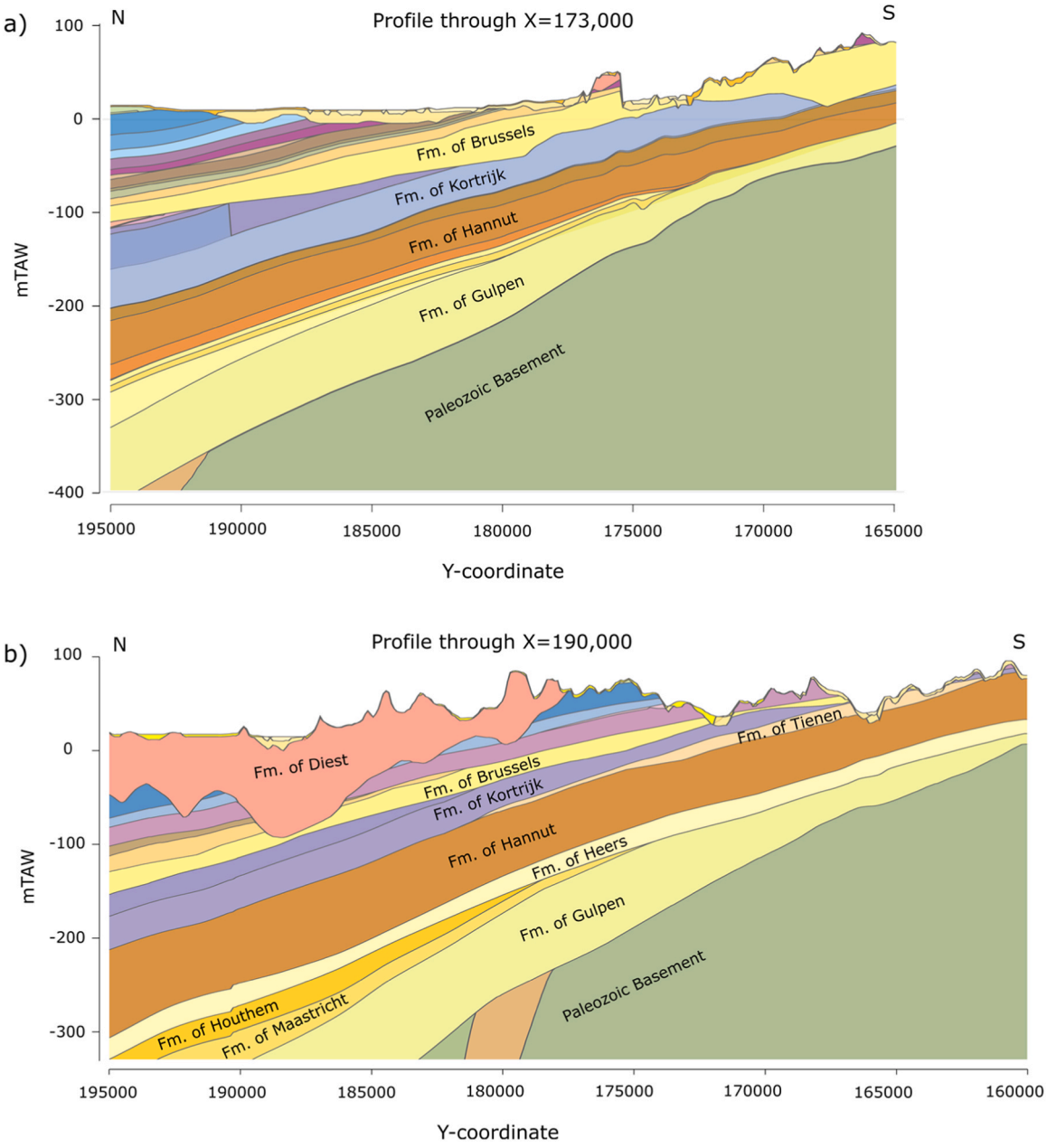

Fig. 4. Geological profiles with vertical exaggeration: a) north-south profile through Leuven area (X = 173,000); b) north-south profile through Tienen area (X = 190,000); profiles adapted from Databank Ondergrond Vlaanderen (DOV), the subsurface database of Flanders. Elevation is given in meters relative to the Second General Levelling (m TAW), the Belgium's official vertical reference system.

Given its complexity, Cretaceous formations are grouped into four main units according to the G3Dv3 model. The first model unit is defined by the Houthem Formation (Early Paleocene). This formation consist of calcareous arenites or tuff chalk, soft sediments with little differentiation from the underlying formations of Maastricht and Kunrade. The Houthem Formation is found in the Roer Valley Graben and the Campine Basin (Fig. 5a).

The second model unit gathers the formations of Maastricht and Kunrade, the former being found exclusively in the Campine basin, the latter in both, the Campine basin and in the Roer Valley Graben (Fig. 5b). The Kunrade Formation at the Roer Valley Graben is equivalent to the western Maastricht Formation. Both formations are primarily composed of coarse limestone arenites, however, the Kunrade Formation contains alternating banks of contrasting hardness. At their lower boundary, glauconite is present.

At the top of the third unit, chalk sediments of the Nevele Formation—the lateral equivalent of the Gulpen Formation—occur along the Brabant massif and southwest Flanders (Fig. 5c). This model unit also includes the Bernissart, Vert Galand, Esplechin, and Maisière Formations in the southern regions of the Brabant Massif; these formations consist of variable deposits such as glauconitic limestone, marls, and chalks, among others. In the Campine Basin, underneath the chalk of the Gulpen Formation, marly sands and silty marls, corresponding to the Vaals Formation, are found. Different members are present in the Gulpen Formation: Lanaye, Lixhe, Vijlen, Beutenaken, and Zeven Wegen. The latter forms the largest part of the Cretaceous deposits in the area. The member of Zeven Wegen consists of white, fine-grained chalk, Lixhe of white fine-grained chalk with extensive silex intervals, and the member of Lanaye consists of very fine calcarenites with extensive silex intervals. Marly sands of the Dorne Formation are located further east of the Campine Basin. However, these formation do not extend further east of the Roer Valley Graben due to inverse faulting (Deckers et al., 2019).

The fourth model unit is composed by the Aachen Formation, consisting of locally organic-rich clays and sandstones, exclusively found in the Campine basin (Fig. 5d). The upper boundaries of the unit are difficult to define given a similar composition with the upper Vaals Formation; on the other hand, its lower boundary is well defined by either Paleozoic or Mesozoic units. In terms of spatial extension among the units, this model unit is the smallest (Table 1).

The model units previously described are a simplification of the sediments forming the Cretaceous. The spatial extent and classification of the Cretaceous deposits in Flanders are much more complex. Fig. 6 displays the lithostratigraphic correlations based on data and information described in more detail in previous studies and literature (Lagrou and Dreesen, 2005, 2011; Deckers et al., 2019; Ghysels and Mustafa, 2021).

As described previously, the complexity of the Cretaceous and its importance in the region makes its characterization critical. In this work, the hydrogeological properties of the Cretaceous are investigated, specifically focused on hydraulic conductivity. The spatial variability of this parameter is investigated with respect to depth and the complex lithology of the Cretaceous in the region of Flanders.

3. Methodology

To evaluate the hydrogeology and physical properties of the Cretaceous, data was collected from several technical studies and hydrogeology reports provided by De Watergroep, the largest public drinking water company in Flanders (De Watergroep, 1978, 1988, 1993, 2001, 2004a, 2004b, 2010, 2013, 2015, 2016, 2017a, 2017b, 2017c, 2017d, 2021). For this study, data from extraction and

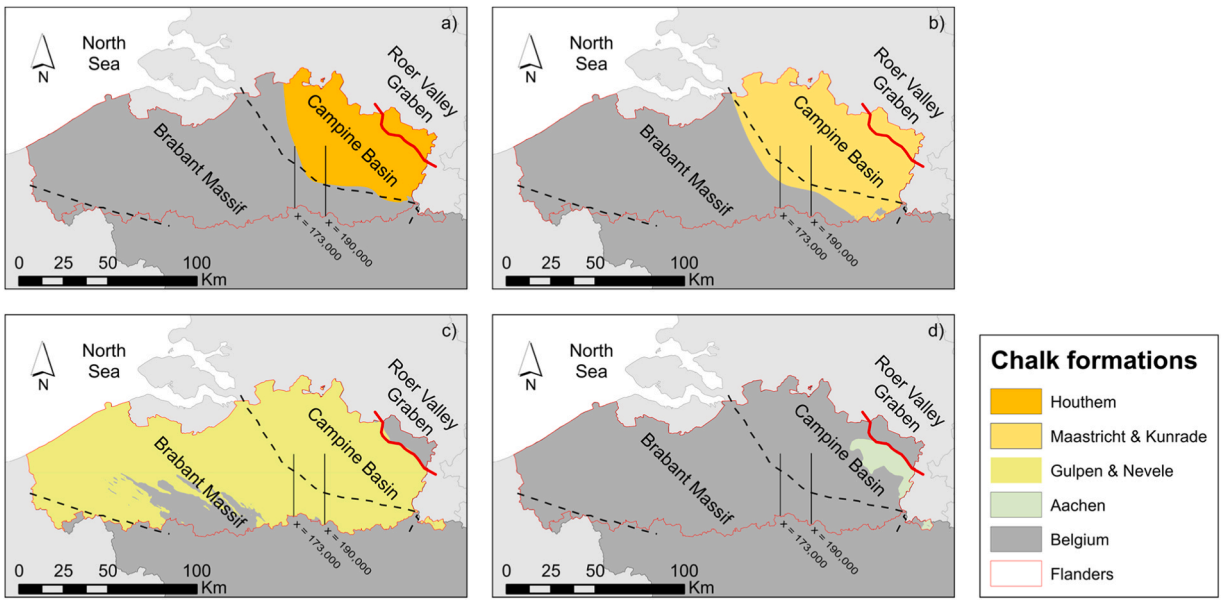

Fig. 5. The Cretaceous' formations in Flanders according to the G3Dv3 model units. Dotted lines indicate boundaries of the Brabant Massif. Red bolt line indicates the edge of the Roer Valley Graben. Continuous black lines indicate the geology cross sections displayed in Fig. 4.

Table 1
Model units of the Cretaceous. Values for the region of Flanders.

Age	Formations	Area (km^2)	Maximum thickness (m)	Top (m TAW)	
				Maximum	Minimum
Danian	Houthem	3763	76	71	−1347
Maastrichtian	Maastricht and Kunrade	5308	93	127	−1411
Maastrichtian, Campanian, Santonian, Coniacian, Turonian, Cenomanian	Gulpen (Nevele, Dorne, Vaals, Bernissart, Vert Galand, Esplechin, and Maisière)	12,303	381	268	−978
Santonian	Aachen	496	71	198	−797

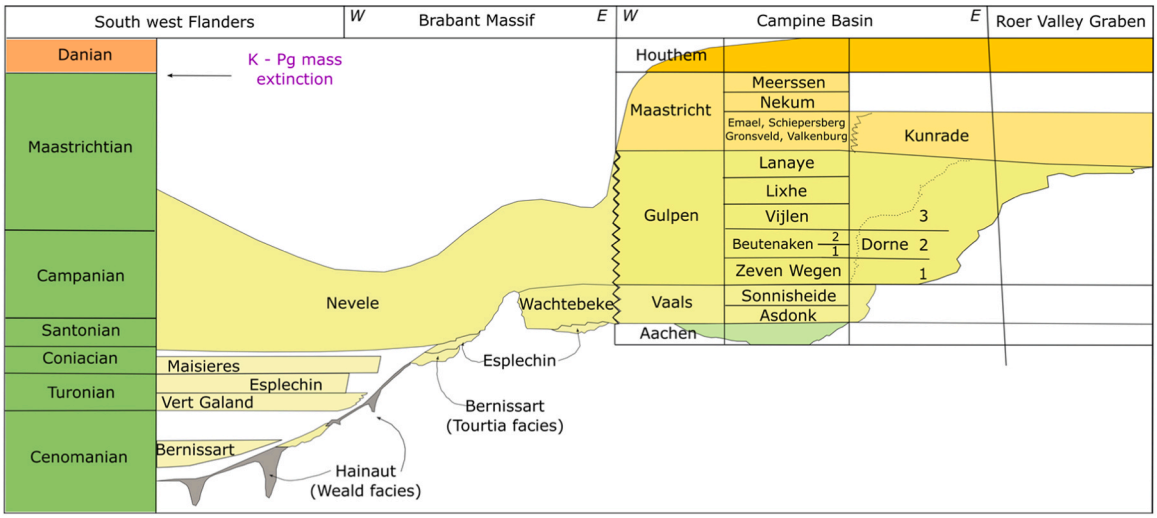

Fig. 6. Lithostratigraphic of the Cretaceous deposits in Flanders (Lagrou and Dreesen, 2011). Modified according to the G3Dv3 model units and colour code.

observation wells, distributed across the provinces of Flemish Brabant and Limburg, were gathered for analysis from the aforementioned reports. For 29 wells, flowmeter logs data were available. To correlate flow rates with the local geology, 23 geophysical logs, such as natural gamma-ray logs, were applied. Further, operational data from De Watergroep provided estimates of the well yields and drilling descriptions defining the aquifer boundaries and thickness (see Appendix A).

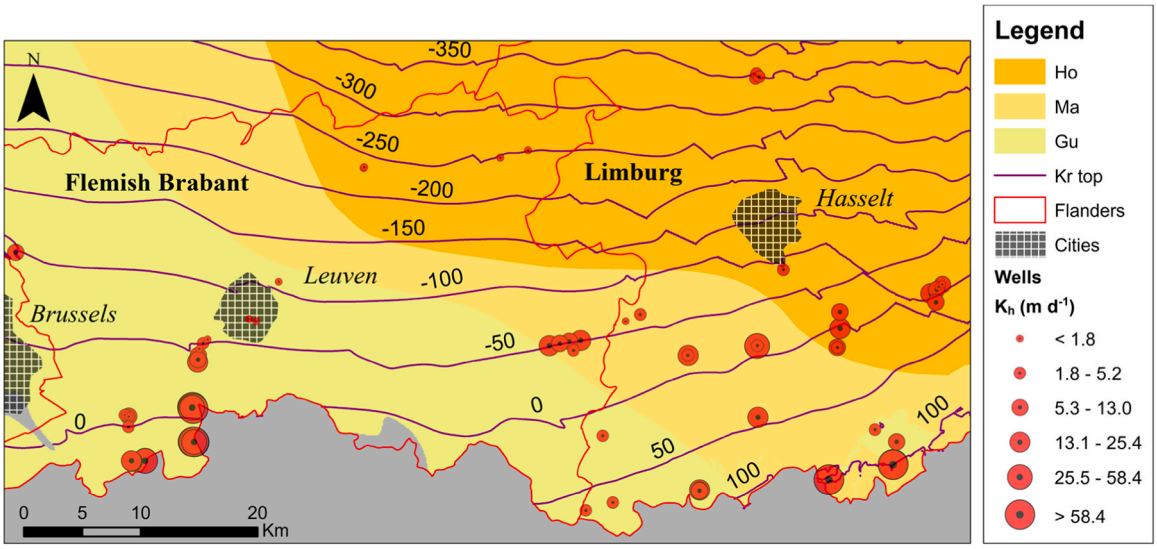

Fig. 7. Wells corresponding to extraction sites utilized in this study. The purple lines indicate the Cretaceous (Kr) top in m TAW. Diameter of the red circles denoting the wells gives an indication of the horizontal hydraulic conductivity.

However, some wells in the dataset were equipped with screens extending significantly into Paleocene aquifer systems (e.g., Hannut Formation) overlying the Cretaceous. Since this work focuses solely on the physical properties of the Cretaceous, such wells were excluded from the analysis to minimize over– or under –estimations. In total, 68 wells located in the Cretaceous are included in this analysis, 30 of which are located in the Flemish-Brabant province. The screens of wells located in the Cretaceous are vertically distributed across the Houthem (Ho), Maastricht (Ma), and Gulpen (Gu) Formations and corresponding units, either penetrating a single formation or a combination of them. Consequently, the depth of the wells and the vertical location of the screens range from tens of metres to approximately −350 m TAW (Fig. 7).

Appendix A1 displays a table containing geographic and technical information about the wells, as well as other important data evaluated in this study. The top and base of the screens were obtained directly from the provided technical reports and hydrogeological studies. The top and bottom of the Cretaceous were derived from the G3Dv3 model. Similarly, the formations supplying water at the extraction sites were also defined by the model according to the work of Ghysels and Mustafa (2021). Elevation data for the well locations were obtained from the Digital Elevation Model Flanders II (DHMV II), which has Root Mean Squared Errors (RMSEs) of approximately 0.10 m and 0.05 m for the x, y, and z axes, respectively, based on a combination of LiDAR data and high-quality aerial images (Digital Flanders Agency, 2014).

Physical parameters such as horizontal hydraulic conductivity (K_h) transmissivity (T), and storage (S) were estimated from 63 pumping tests. Each pumped test was interpreted using analytical solutions and/or numerical models, depending on the complexity of the hydrogeology, the well conditions, and the purpose and timing of the test. The methods employed included the Theis method (Theis, 1935), Theis-Jacob method (Jacob, 1947), Cooper-Jacob method (Cooper and Jacob, 1946), and Hantush method (Hantush and Jacob, 1955). Each method was applied based on the hydrogeological conditions of the wells and the stage of drawdown. After applying the corresponding equations of each method to obtain T, K_h was derived from:

$$K_h = T * b^{-1} \tag{1}$$

were K_h is the horizontal hydraulic conductivity in m day^{-1}, T is the transmissivity in m^2 day^{-1}, and b is the saturated thickness of the aquifer in metres. Additionally, T and K_h were also estimated using numerical simulations of the pumping tests with MODFLOW (Harbaugh, 2005) and the Multi-Layered approach or MLU (Hemker, 1999; Hemker and Post, 2013). MODFLOW is a three-dimensional finite-difference groundwater model capable of simulating aquifer layers (confined, unconfined, or combined) with steady and unsteady flow, while MLU is suitable for building fully three-dimensional analytical models of transient well flow in layered aquifer systems. For some wells, multiple pumping tests were performed at different stages, or multiple methods of analysis were used to estimate physical parameters. In these cases, an average K_h value was determined for such wells.

Given that K_h—the dependent variable in this analysis—was estimated from pumping tests, potential predictor variables, related to well characteristics and locations, were also included to investigate their possible influence on K_h. Therefore, the predictor variables for this study, in addition to the different lithology formations, are: Cretaceous depth (or top of the Cretaceous), Cretaceous thickness, and screen length. In addition to the descriptive statistics presented in the following sections, Pearson correlation coefficients were calculated to investigate the covariance among the dependent variable and the predictor variables by:

$$r = \frac{\Sigma_{i=1}^{n} (x_i - \overline{x})(y_i - \overline{y})}{\sqrt{\Sigma_{i=1}^{n} (x_i - \overline{x})^2 \Sigma_{i=1}^{n} (y_i - \overline{y})^2}} \tag{2}$$

were x_i and y_i are the corresponding values for the dependent and predictor variables; $\bar{x}$ and $\bar{y}$ are the means of the analysed variables, and n is the number of data points. Also, given the nature of the data and the numerical ranges they display, logarithmic models were tested. Residual analysis was used to evaluate the goodness of fit and the assumptions of the regression models, serving to identify influential data points (outliers) greater than two standard deviations at the different stages of the correlation analysis.

4. Results and discussion

4.1. Trends between K_h, lithology, and the predictor variables

A descriptive analysis indicated that K_h varies widely, ranging from 0.13 to 173 m day^{-1}. This variation, spanning several orders of magnitude, was expected given the characteristics of the Cretaceous. Although the intrinsic uncertainty derived from the K_h estimation process should not be overlooked, this variation is congruent with the high heterogeneity of this aquifer. According to well locations, Cretaceous depth ranges from just few metres below the surface to depths exceeding 280 m, while its thickness ranges from 17 m to approximately 250 m. Minimum and maximum values for screen length range from 8 to 80 m, respectively.

To investigate the range of K_h and the variability of the predictor variables within and across the different geological formations, these variables were grouped according to the formations intersected by the well screens. The notable K_h variability is displayed not only among the different formations but also within a specific formation. The Gulpen Formation exhibits a wider range in which K_h spans three orders of magnitude. In contrast, in the Maastricht Formation, or combinations including it, K_h shows a moderate variability with more homogeneous values and a spread falling withing the same order of magnitude. The spread of K_h per formation demonstrates an interesting trend, decreasing as formations go deeper. This is also reflected in the average K_h values per formation displaying a similar trend, with the K_h average of the Gulpen Formation being the highest while that of the Houtem Formation, found in deeper northern regions, displays the lowest (Table 2). It is important to point out that, these values reflect the characteristics at the

well's location and screens vertical position only.

Notably, the Gulpen maximum and minimum K_h values align with those observed in the descriptive analysis. This suggest that the Gulpen Formation could play a significant role in driving most of the variability in estimated K_h, most likely due to the contrasting levels of weathering, fracturing, and lithology heterogeneity. This is better displayed in Fig. 8a, in which a noteworthy decrement of up to two orders of magnitude for screens crossing the Houthem and Maastricht formations compared to those exclusively crossing the Gulpen Formation is visualized.

The predictor variables also display interesting trends in relation to the formations. For the Cretaceous depth, the Gulpen Formation presents shallower depths with an average of approximately 38 m (Fig. 8b). In addition to the lithology of the Gulpen Formation, which intrinsically presents high K_h values, the shallowness of this formation in southern areas could also explain even higher values for K_h due to the proximity to the surface, and hence, greater exposure to weathering processes. On the other hand, the depth this formation reaches at the south could also influence a decrement in K_h due to an increasing overburden pressure affecting fracturing development due to compression. Depths for the combined Maastricht and Gulpen Formations display similar spreads, with a mean value of approximately 107 m. Wells crossing simultaneously Houthem and Maastricht Formations are also located in northern areas and are the deepest wells from the dataset. Notably, the Cretaceous depth for these wells, correlate with the lower averaged K_h values displayed in Fig. 8a. Cretaceous depth is not uniform across the wells locations.

The Cretaceous thickness varies across formations, with a general tendency to increase northward alongside with depth. Fig. 8c shows that, according to the wells location in this study, screens crossing simultaneously Houthem and Maastricht formations correspond to the thickest Cretaceous section, while those located at the Gulpen Formation correspond to the thinnest. The southern wells of Heusden supported this trend in accordance to ranges presented by Cretaceous depth and the cross sections presented in Fig. 4.

The screen length displayed a pronounced variability across the formations without a noticeable trend. This could be the result of adaptations made according to the hydraulic and geological conditions of the extractions sites or specific well designs optimized for groundwater extraction. Unlike the previous predictor variables, screen length did not display a clear trend in relation to the formations they cross.

For the Cretaceous in general, some interesting trends between the variables and the formations were observed. However, the most notables were the inverse relations between K_h and predictors Cretaceous depth and Cretaceous thickness. To explore further these trends, a correlation analysis followed.

4.2. Correlation and residual analysis

An initial analysis indicated fairly moderate correlations for K_h with the predictor variables Cretaceous depth and Cretaceous thickness (Table 3). Although moderate, the negative Pearson correlation coefficients (r) indicates a decrease in K_h as the depth and the thickness of the Cretaceous increased; there is a strong positive correlation between the depth and thickness of the Cretaceous.

The proportions of variance explained by the predictors Cretaceous depth, Cretaceous thickness, and screen length were very low, with coefficients of determination (R^2) of 0.15, 0.10, and 0.07, respectively. To evaluate the suitability of the predictor variables for transformations, density plots and histograms were used to explore the distribution of these variables across the wells. Fig. 9 displays a right-skewed distribution for K_h (a) indicating possible effects on linear modelling due to the lack of normality; the predictors Cretaceous depth (b), Cretaceous thickness (c), and screen lenght (d) displayed possible bimodal distributions sugesting distinct groups of clusters.

To deal with the non normality and potential high outliers, a logaritmic transformation was carried out for the dependent variable K_h. No transformation was attempted for the predictor variables given the bimodal or multimodal nature of the data, characteristics not fully addressed by transformations. An initial model for the Cretaceous aquifer as a whole was developed by including all K_h values from all observations, regardless of formation.

First, the fitted logarithmic regression revealed a weak correlation between K_h and the Cretaceous depth, with a coefficient of determination of 0.31, despite an apparent trend (Fig. 10a). Residual analysis showed some heteroscedasticity; outliers, extending more that two standard deviations, influencing the correlation were identified (Fig. 10b). However, excluding these outliers resulted in minimal improvement to the model (Fig. 10c).

Correlations with predictors Cretaceous thickness and screen length displayed R^2 values of less than 0.19. Therefore, these predictor variables were excluded from further analysis, being Cretaceous depth the sole potential predictor for K_h in further analysis.

Logarithmic models were tested for each of the formations. In Fig. 11a, 35 observations from the Gulpen Formation showed a fairly strong negative correlation between K_h and the depth of the Cretaceous, following a logarithmic decay pattern as the Cretaceous top deepens. It is important to highlight the influence of hardground layers embedded in this formation and the low permeability of the

Table 2
Maximum, mean, and minimum K_h (m d^{-1}) values according to intersected formations.

Value	Formations				
	Ho/Ma	Ho/Ma/Gu	Ma/Gu	Ma	Gu
Minimum	1.00	0.76	1.72	1.88	0.13
Geometric mean	1.41	3.77	4.71	5.24	11.68
Maximum	2.00	17.52	35.42	19.43	173
Number of wells	2	14	8	9	35

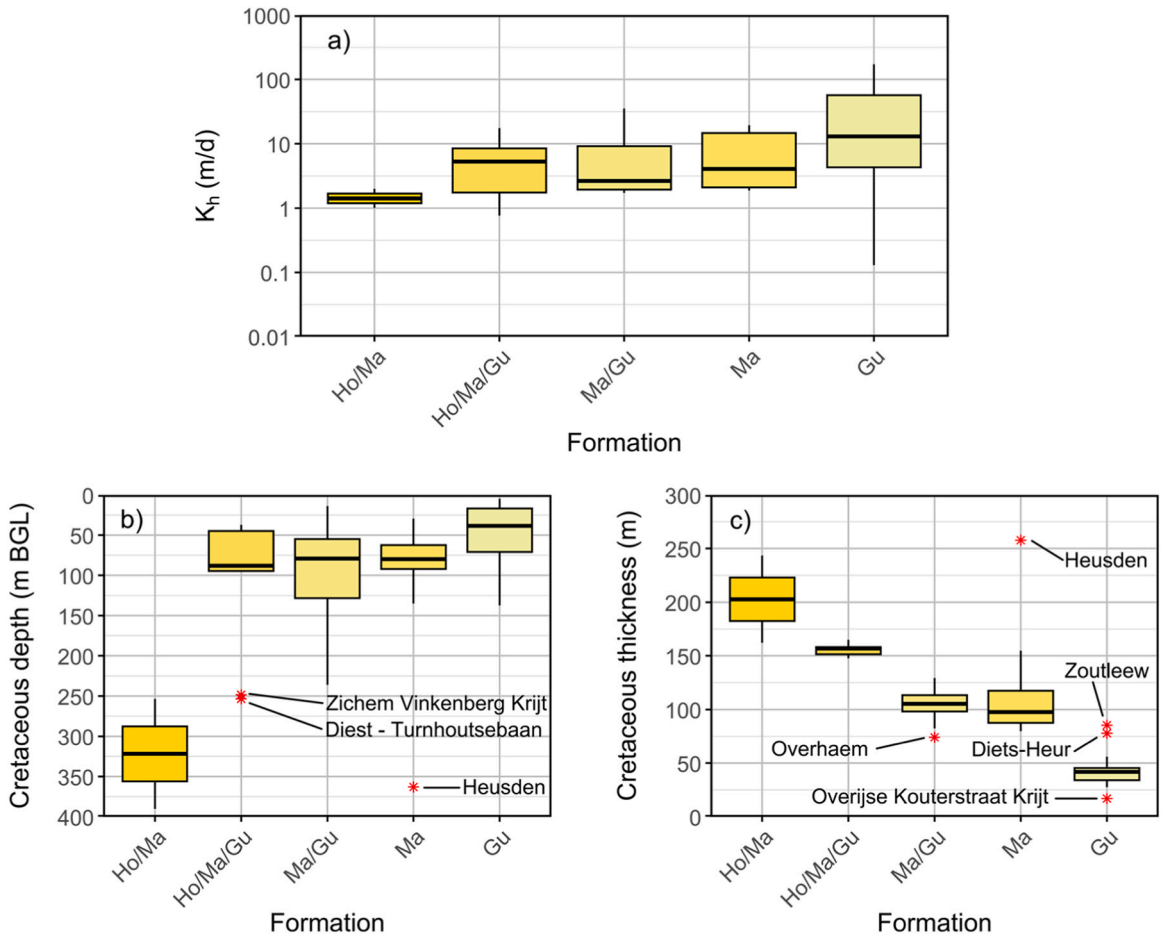

Fig. 8. Dependent and predictor variables in correspondence to the intersected formations.

Table 3
Pearson correlation coefficients between K_h and the predictor variables.

	K_h	Cretaceous depth	Cretaceous thickness	Screen length
K_h	1	−0.387	−0.315	−0.278
Cretaceous depth	−0.387	1	0.654	0.376
Cretaceous thickness	−0.315	0.654	1	0.528
Screen length	−0.278	0.376	0.528	1

Zeven Wegen member. Residual analysis displayed a single outlier possibly influencing the correlation (Vilvoorde Drie fonteinen) and a non-constant variance of residuals (Fig. 11b). Outlier exclusion improved the model's accuracy indicating a fairly stronger correlation between these two variables (Fig. 11c). Intercept and slope for this model remained statistically significant with P values of less than 0.05.

Similar analysis was performed on the combined formations of Houthem, Maastricht, and Gulpen, resulting in fairly moderate negative correlations. Nevertheless, during the residual analysis for each of them, no outliers were found. This could be the consequence of the range of observed K_h values and the smaller number of observations per individual formation, not allowing model improvement. Therefore, to avoid misrepresentations on the models, the remaining K_h measurements corresponding to these formations were evaluated together. As displayed in Fig. 11d, the initial model showed a fairly moderate correlation with notable outliers at deeper sections of the aquifer, resulting in a steeper negative slope in comparison to that from the Gulpen model. The residual analysis indicated a more pronounced heterocedasticity compared to that from the Gulpen model, suggesting more inconsistent errors in the model (Fig. 11e). After excluding the outliers, the model displayed a moderate improvement (Fig. 11f).

The fitted models support the hypothesis that a correlation between K_h and the Cretaceous depth exists. Solving the logarithmic equations for K_h, we derived from the models:

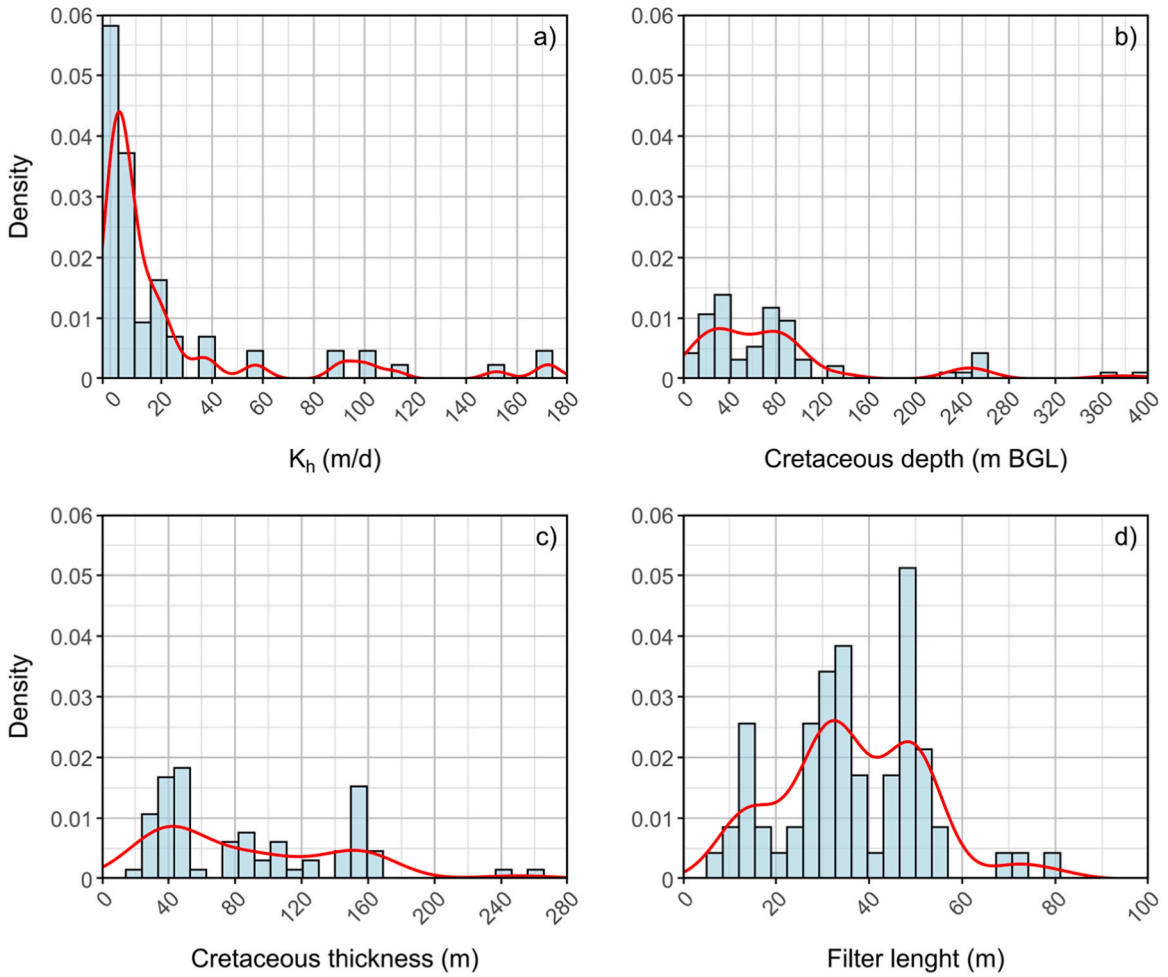

Fig. 9. Histograms and density plots of the variables.

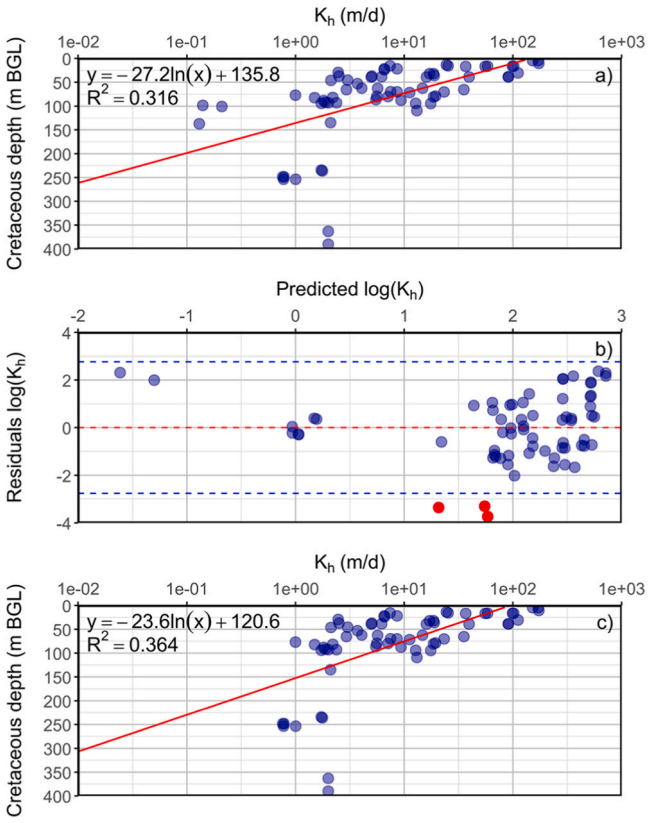

Fig. 10. Initial model, residual analysis, and fitted model for the Cretaceous aquifer (all formations). Red dots represent outliers greater than two standard deviations (blue dashed lines).

$$K_h = e^{\frac{d-78.4}{-13.4}} \quad (3)$$

and

$$K_h = e^{\frac{d-169.9}{-45.5}} \quad (4)$$

where Eq. (3) and Eq. (4) correspond to the models for the formations of Gulpen and the combination of Houthem, Maasctricht, and Gulpen, respectively. In both equations, d is the Cretaceous depth (m) and e is the inverse of the natural logarithm. The Gulpen Formation model indicates high K_h values at shallower regions in comparison with deeper sections located at north (Fig. 12).

Notwithstanding the considerable strength of the models, it is important to always consider the lithological variability and the intrinsic karstic nature of the Cretaceous when analysing the correlation between K_h and this aquifer's depth. As part of the lithological variability, hardground intervals are present across the study area. These hardground layers, characterized as branched glauconite-bearing bioturbations, at least partially cemented with phosphate cement, display differences in thickness and permeability which influence significantly the spatial variability of K_h. The influence of the hardground on K_h is very different from site to site in the study area. For example, near to Leuven, the hardground layer has demonstrated through previous studies to limit well yields due to its lower permeability of approximately 2 m day^{-1}. In contrast, in southern regions, where the thickness of the hardground increases significantly (e.g., Het Broek, Venusberg, and Geuzenhoek wells), permeability increases up to 140 m day^{-1}. The higher permeability displayed by these hardground, could be explained by the presence of a phospatic gravel deposit derived from a stronger erosion and redeposition of chalk material that underwent reworking or even karstification processes. Although the hardground itself has low permeability, in some areas it serves as an inception horizon for processes on carbonate sediments right above the hardground, which result in in horizons with higher hydraulic conductivity.

The intrinsic composition of the formations and members also influence the variability in K_h. Geophysical and flow measurements indicate that Lixhe and Lanaye, upper members of the Gulpen Formation, provide minor contributions to flow in the north but become more significant in southern regions where they dominate groundwater flow alongside Maastrichtian calcarenites. Similarly, the Zeven Wegen chalk, the lowest member of the Gulpen Formation underlying Lixhe and Lanaye, also hold a very low permeability in northern areas, and contributes with little to no flow (Fig. 13).

Measurements in southern wells demonstrate higher permeabilities which are reflected in higher well yields. These higher permeabilities are the consequence of fracture zones within this chalk member. Therefore the correlation between K_h and depth of

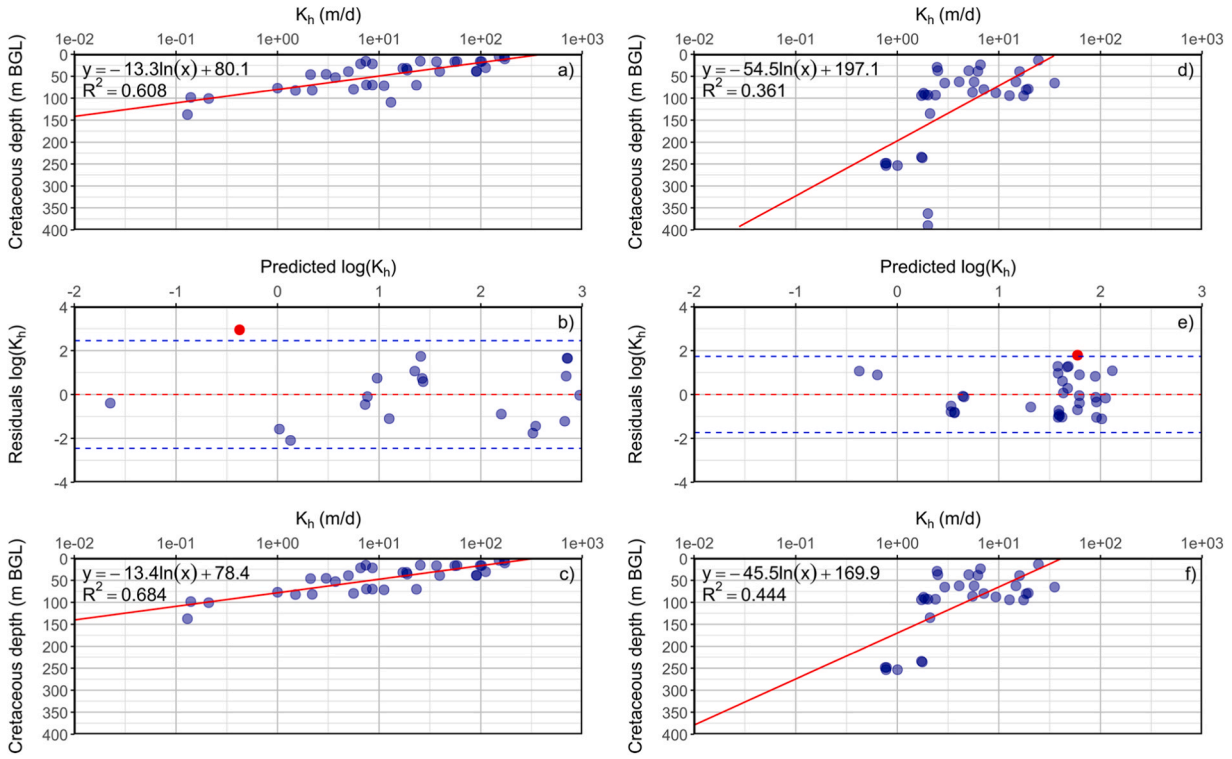

Fig. 11. Initial model, residual analysis, and fitted model for the Gulpen Formation (a, b, and c), and that combining Houthem, Maastricht and Gulpen formations (d, e, and f). Red dots represent outliers greater than two standard deviations (blue dotted lines).

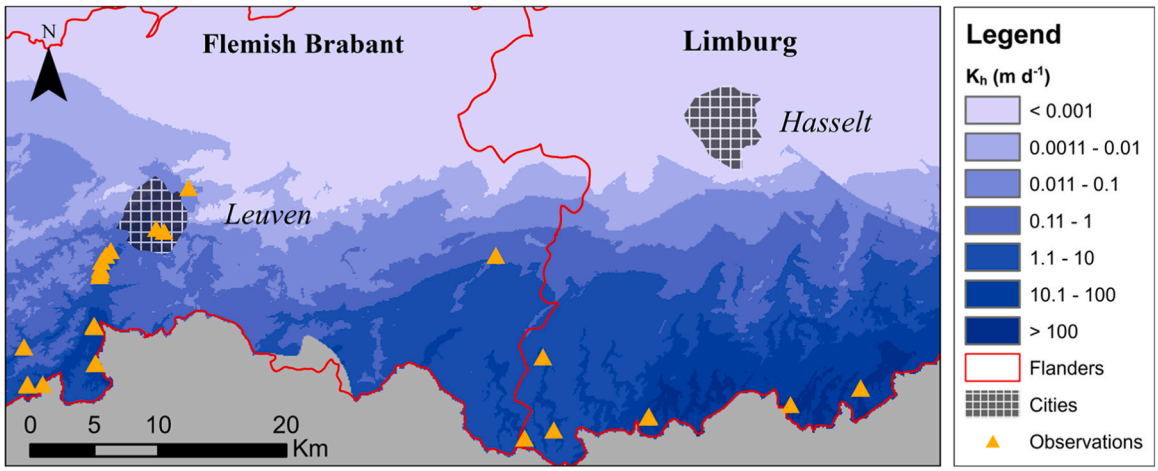

Fig. 12. Spatial variability of K_h according to the Gulpen model.

Cretaceous includes both the presence and permeability of the hardground/phosphatic gravel interval and the effect of fractures. Regarding the latter, in the southern part of the study area, where the Cretaceous is closer to the surface, the chalk is fractured, resulting in a strong increase of hydraulic conductivity. This increase in fracture density is possibly related to the decrease in pressure due to the exhumation of overlying layers. On the other hand, towards the north, where the Cretaceous is deeper in the subsurface, these fractures are not observed, resulting in a much lower hydraulic conductivity.

These outcomes underscore the importance of both, lithological and structural factors in controlling groundwater flow and K_h within the Cretaceous aquifer. In other words, it is necessary to always consider not only the karstic nature of the aquifer, but also the effect of multiple lithologies being evaluated together, in addition of inherent randomness when further evaluating the proposed models.

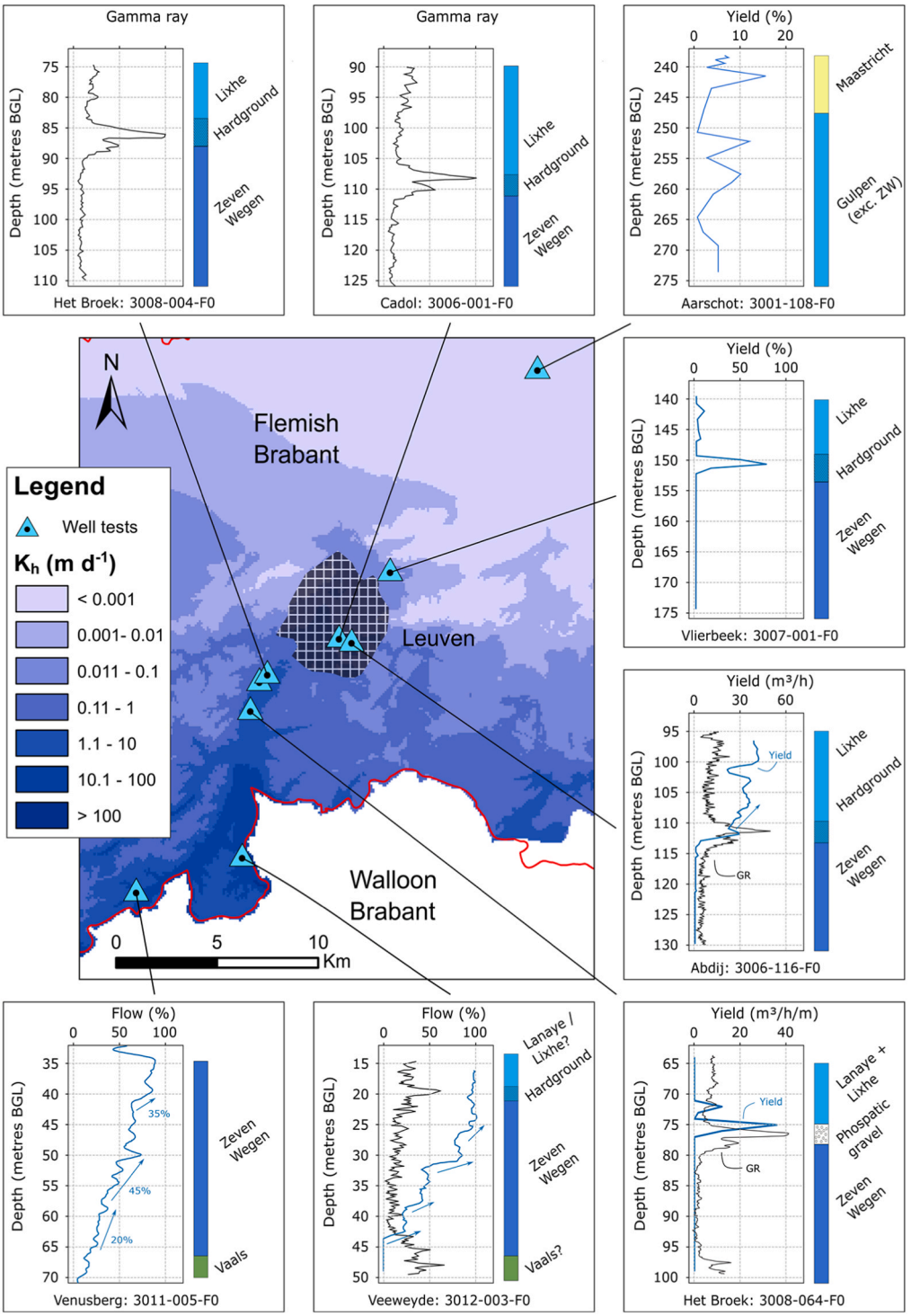

Fig. 13. Stratigraphy, flowmeter log, and natural gamma-ray log of some of the wells in the study area. Modified from Ghysels and Mustafa (2021).

5. Conclusions

In Flanders, the Cretaceous aquifer is a very important source of water supply for drinking water, agriculture, and industry. However, in order to investigate the capacity of the Cretaceous for the implementation of exploitation or preservation strategies, it is necessary to gain further knowledge on the spatial distribution of the Cretaceous' physical and hydraulic properties.

In this study, statistical analysis and regression models were applied to characterize the Cretaceous in terms of K_h based on data from extraction and monitoring wells. Results indicate that a negative correlation between K_h and the Cretaceous depth exists. Two models were estimated to represent this correlation, the first one to represent the Gulpen Formation and the second one as a combination of Houthem, Maastricht, and Gulpen Formations.

Models indicate that, as the Cretaceous dips towards the north, K_h decreases even by several orders of magnitude in comparison with southern locations where the Cretaceous is closer to the surface. This spatial variability of K_h, and the correlation it displays with the Cretaceous depth, is driven by lithology differences and highly permeable layers of hardground and phosphatic gravels embedded in the Gulpen Formation. This hardground, plays an important role for some extraction sites as its permeability is also related with its thickness and depth. The significant increase in K_h in southern areas could be interpreted as an expression of karstification and weathering processes. Being more exposed to the surface and likely due to a decrease in pressure from the exhumation of overlying layers, chalk formations present a higher fracture density at the south in comparison to northern areas. Therefore, the spatial variability of K_h in the Cretaceous is driven by the combined impact of lithology, fracture density, karstification processes, and depth. The models here presented, can be implemented into numerical groundwater flow models in order to evaluate optimal groundwater extraction volumes, secure future water demand scenarios, maximize the storage capacity (e.g., Managed Aquifer Recharge), or the implementation of strategies to minimize the negative effects of climate change (e.g., Aquifer Thermal Energy Storage). Nevertheless, for future works or use of the models, we suggest the following considerations:

- The Gulpen Formation displays the higher K_h variability by four orders of magnitude.
- Fractures and permeable hardground layers play an important role for the Gulpen K_h.
- Important to consider the logarithmic nature of the model, since small deviations could lead to significant under- or overestimations.
- The models are based on K_h estimates, which inherently carry certain degree of uncertainty due to the method of estimation.

The models presented in this work provide novel information on the Cretaceous trends, suggesting interesting initial conditions to be further tested for model improvement.

CRediT authorship contribution statement

Miguel Moreno Gómez: Writing – original draft, Methodology, Investigation, Data curation, Visualization, Formal analysis. **Gert Ghysels:** Writing – original draft, Investigation, Formal analysis, Data curation. **Syed M. T. Mustafa:** Writing – original draft, Investigation, Formal analysis, Data curation. **Simon Six:** Review & editing, Supervision. **Alexander Vandenbohede:** Review & editing, Supervision. **Tom Diez:** Review & editing, Supervision. **Dirk Gijsbert Cirkel:** Review & editing, Validation, Supervision. **Marijke Huysmans:** Review & editing, Validation, Supervision.

Funding

This work was partially funded by the project "CHalk AquifeR Management (CHARM): Analysing the capacity of the Cretaceous Aquifer in Brabant, Belgium" project n° 402045.068, and the project "*Accelerating and mainstreaming transformative NATure-bAsed solutions to enhance resiLIEence to climate change for diverse bio-geographical European regions*" (https://www.natalieproject.eu/), funded by the European Union, the UK Research and Innovation and the Switzerland Federal Department of Economic Affairs Education and Research; grant agreement n° 101112859.

Declaration of Competing Interest

The authors declare that they have no known competing financial interests or personal relationships that could have appeared to influence the work reported in this paper.

Acknowledgments

The authors of this work would like to thank De Watergroep for the data provided to carry out this work and the support of KWR.

Appendix A1. Data utilized in this work. (HS = Hydrogeological study; TR = Technical report; PT = Pumping test; P2, P3 = Monitoring wells; Kr = Cretaceous)

ID	X	Y	Province	Extraction Site	Source	Type	Well	Elevation (m TAW)	Formation	Kr Top	Kr Base	Kr Thickness	Kh (m/d)	Filter Top	Filter Base	Filter Length
1	183511	185746	Vlaams-Brabant	Aarschot Krijt (Schoonhoven)	HS	PT	3001–107	14.4	Ma/Gu	234.2	342.1	107.9	1.73	238.0	253.0	15.0
2	183464	185677	Vlaams-Brabant	Aarschot Krijt (Schoonhoven)	HS/TR	PT	3001–108	16.4	Ma/Gu	236.0	343.1	107.1	1.76	236.4	276.4	40.0
3	197522	187198	Vlaams-Brabant	Diest - Turnhoutsebaan	HS	PT	3002–025	23.5	Ho/Ma	253.5	415.6	162.1	1.01	270.0	315.0	45.0
4	197535	187210	Vlaams-Brabant	Diest - Turnhoutsebaan	HS	PT	3002–026	23.5	Ho/Ma/Gu	253.5	415.6	162.1	0.78	268.0	348.0	80.0
5	195137	186548	Vlaams-Brabant	Zichem Vinkenberg Krijt	TR	PT	3002–028	21.1	Ho/Ma/Gu	248.4	406.5	158.1	0.78	271.0	343.0	72.0
6	195141	186547	Vlaams-Brabant	Zichem Vinkenberg Krijt	TR	PT	3002–031	21.1	Ho/Ma/Gu	248.4	406.5	158.1	0.76	265.0	321.0	56.0
7	173644	172757	Vlaams-Brabant	Heverlee Cadol	HS	PT	3006–001	24.4	Gu	98.4	130.6	32.2	0.14	96.3	126.0	29.8
8	174276	172561	Vlaams-Brabant	Heverlee Abdij	HS	PT	3006–116	27.6	Gu	100.8	134.6	33.8	0.21	99.7	132.0	32.4
9	176177	175954	Vlaams-Brabant	Kessel-lo Vlierbeek	HS/TR	PT	3007–001	24.7	Gu	137.3	183.0	45.7	0.13	142.0	179.0	37.0
10	169223	169076	Vlaams-Brabant	Korbeek Dijle Het Broek	HS	PT	3008–001	26.6	Gu	70.3	110.7	40.4	23.30	72.0	108.0	36.0
11	169373	170207	Vlaams-Brabant	Korbeek Dijle Het Broek	HS	PT	3008–002	35.4	Gu	82.3	124.2	41.9	1.50	77.0	111.0	34.0
12	169696	170670	Vlaams-Brabant	Korbeek Dijle Het Broek	HS	PT	3008–003	30.6	Gu	81.8	116.2	34.4	2.20	78.0	113.0	35.0
13	170091	171033	Vlaams-Brabant	Korbeek Dijle Het Broek	HS	PT	3008–004	24.4	Gu	77.1	109.6	32.5	1.00	80.0	110.0	30.0
14	169298	169638	Vlaams-Brabant	Korbeek Dijle Het Broek	HS	PT	3008–005	27.1	Gu	70.0	117.4	47.4	8.60	68.0	119.0	51.0
15	169280	169513	Vlaams-Brabant	Korbeek Dijle Het Broek	HS	PT	3008–006	28.3	Gu	71.6	117.8	46.2	11.20	66.0	111.0	45.0
16	169259	169286	Vlaams-Brabant	Korbeek Dijle Het Broek	TR	PT	3008–064	26.1	Gu	69.8	112.9	43.1	7.50	68.0	102.0	34.0
17	163297	163520	Vlaams-Brabant	Overijse Kouterstraat Krijt	TR	PT	3010–001	52.6	Gu	52.9	69.9	17.0	3.71	51.7	67.5	15.8
18	163610	160562	Vlaams-Brabant	Overijse Venusberg Krijt	TR	PT	3011–005	58.3	Gu	36.0	80.0	44.0	18.90	31.8	67.8	36.0
19	163583	160581	Vlaams-Brabant	Overijse Venusberg Krijt	TR	PT	3011–006 (P2)	54.1	Gu	32.0	75.9	43.9	18.60	32.0	40.0	8.0
20	163555	160607	Vlaams-Brabant	Overijse Venusberg Krijt	TR	PT	3011–007 (P3)	54.1	Gu	32.0	75.9	43.9	17.10	35.0	45.0	10.0
21	164745	160598	Vlaams-Brabant	Overijse Sana Tombeek	HS	PT	3011–008	38.6	Gu	16.8	54.1	37.3	36.79	23.9	51.4	27.5
22	164746	160626	Vlaams-Brabant	Overijse Sana Tombeek	HS	PT	3011–009	38.6	Gu	16.8	54.1	37.3	55.55	26.0	40.0	14.0
23	168889	162233	Vlaams-Brabant	St.-Agatha Rode Veeweyde	HS	PT	3012–001	36.6	Gu	16.4	47.7	31.3	98.83	21.0	52.0	31.0
24	168936	162225	Vlaams-Brabant	St.-Agatha Rode Veeweyde	HS	PT	3012–002	36.6	Gu	16.4	47.7	31.3	101.84	17.9	48.4	30.5

(*continued on next page*)

(*continued*)

ID	X	Y	Province	Extraction Site	Source	Type	Well	Elevation (m TAW)	Formation	Kr Top	Kr Base	Kr Thickness	Kh (m/d)	Filter Top	Filter Base	Filter Length
25	168845	162230	Vlaams-Brabant	St.-Agatha Rode Veeweyde	HS	PT	3012–003	49	Gu	30.5	58.1	27.6	111.70	23.6	46.4	22.8
26	168841	165088	Vlaams-Brabant	St.-Agatha Rode Geuzenhoek	HS	PT	3012–007	29.1	Gu	38.6	76.3	37.7	90.41	35.3	72.3	37.0
27	168789	165194	Vlaams-Brabant	St.-Agatha Rode Geuzenhoek	HS	PT	3012–008	28.1	Gu	38.7	76.1	37.4	91.04	41.3	72.0	30.7
28	168758	165170	Vlaams-Brabant	St.-Agatha Rode Geuzenhoek	TR/HS	PT	3012–009 (P3)	28.5	Gu	38.9	76.8	37.9	39.48	48.0	77.0	29.0
29	168917	162226	Vlaams-Brabant	St.-Agatha Rode Veeweyde	TR	PT	3012–059	36.6	Gu	16.4	47.7	31.3	58.40	18.3	47.5	29.2
30	153662	178449	Vlaams-Brabant	Vilvoorde 3 fonteinen	TR	MLU	3014–004	8.8	Gu	109.4	143.0	33.6	13.08	115.8	145.0	29.2
31	200236	170663	Limburg	Zoutleew	HS	PT	3018–001	27.8	Gu	79.7	165.1	85.4	5.60	85.6	155.7	70.2
32	199332	170470	Limburg	Zoutleew	HS	PT	3018–003	29	Ma	80.7	163.2	82.5	18.60	80.0	94.0	14.0
33	201054	170834	Limburg	Zoutleew	HS	PT	3018–004	28.5	Ma	80.0	167.5	87.5	7.10	79.5	94.5	15.0
34	202025	170907	Limburg	Zoutleew	HS	PT	3018–005	28.1	Ma	79.0	168.6	89.6	19.43	82.0	94.5	12.5
35	207118	173122	Limburg	Nieuwerkerken	TR	PT	4009–001 (P1)	33.7	Ma/Gu	93.0	222.4	129.4	2.01	105.2	158.2	53.0
36	207128	173128	Limburg	Nieuwerkerken	TR	PT	4009–002	33.7	Ma/Gu	93.0	222.4	129.4	2.38	105.5	160.0	54.5
37	211225	169631	Limburg	Zepperen	TR	PT	4010–001	42.7	Ma	62.5	160.2	97.7	14.73	69.5	119.0	49.5
38	211202	169649	Limburg	Zepperen	TR	PT	4010–002	42.7	Ma	62.5	160.2	97.7	4.07	69.0	119.0	50.0
39	217133	170447	Limburg	Wellen	TR	PT	4011–001 (P1)	50.2	Ma/Gu	65.4	168.9	103.5	35.42	71.0	121.5	50.5
40	217145	170464	Limburg	Wellen	HS	PT	4011–002	50.2	Ma/Gu	65.4	168.9	103.5	2.94	72.0	125.0	53.0
41	224210	173349	Limburg	Vliermaalroot	HS	PT	4012–001	43.2	Ho/Ma/Gu	62.7	221.7	159.0	5.70	59.5	108.0	48.5
42	223993	170318	Limburg	Vliermaal	HS	PT	4012–010	57.1	Ho/Ma/Gu	38.5	186.1	147.6	6.20	44.6	94.1	49.5
43	223998	170306	Limburg	Vliermaal	HS	PT	4012–011	56.5	Ho/Ma/Gu	37.2	185.6	148.4	5.05	50.0	98.0	48.0
44	223998	170306	Limburg	Vliermaal	TR	PT	4012–011 (P2)	56.5	Ho/Ma/Gu	37.2	185.6	148.4	2.51	50.0	98.0	48.0
45	233007	175731	Limburg	Waltwilder	HS/TR	PT	4013–002 (P2)	53	Ho/Ma/Gu	94.2	251.9	157.7	1.73	106.8	156.5	49.7
46	232666	175521	Limburg	Waltwilder	HS/TR	PT	4013–003 (P3)	51	Ho/Ma/Gu	88.3	243.9	155.6	1.81	106.5	156.0	49.5
47	232433	174171	Limburg	Waltwilder	HS	PT	4013–005	59.9	Ho/Ma/Gu	86.4	238.0	151.6	5.50	103.3	153.3	50.0
48	232500	175267	Limburg	Waltwilder	HS	PT	4013–008	51.9	Ho/Ma/Gu	87.7	240.4	152.7	9.35	100.0	148.0	48.0
49	232002	174926	Limburg	Waltwilder	TR	PT	4013–009	60.9	Ho/Ma/Gu	94.7	246.0	151.3	17.53	100.8	125.8	25.0
50	233001	175701	Limburg	Waltwilder	TR	PT	4013–019	53	Ho/Ma/Gu	94.2	251.9	157.7	12.73	102.0	121.0	19.0
51	203920	162748	Limburg	St. Truiden Velm Krijt	HS	PT	4015–001	62.4	Gu	45.5	101.5	56.0	3.01	48.6	96.0	47.4
52	217209	164337	Limburg	Voort (Borgloon)	HS	PT	4017–001	57.1	Ma/Gu	13.7	96.1	82.4	24.47	17.0	54.0	37.0
53	202478	156386	Limburg	Montenaken Zevenbronnen Krijt	HS	PT	4018–007	104.1	Gu	39.2	78.4	39.2	4.99	42.9	75.9	33.0
54	204774	157044	Limburg	Montenaken Zevenbronnen Krijt	HS	PT	4018–008	112.3	Gu	46.1	94.4	48.3	2.12	43.5	77.0	33.5
55	212171	158046	Limburg	Rukkelingen Loon-Bovelingen	HS	PT	4020–001	103.8	Gu	21.8	67.0	45.2	8.60	18.6	52.0	33.4
56	212187	158067	Limburg	Rukkelingen Loon-Bovelingen	HS	PT	4020–002	103.8	Gu	21.8	67.0	45.2	6.57	26.0	54.0	28.0
57	212209	158105	Limburg	Rukkelingen Loon-Bovelingen	TR	PT	4020–003 F1	97.9	Gu	15.6	60.5	44.9	7.40	18.0	32.0	14.0

(*continued on next page*)

(*continued*)

ID	X	Y	Province	Extraction Site	Source	Type	Well	Elevation (m TAW)	Formation	Kr Top	Kr Base	Kr Thickness	Kh (m/d)	Filter Top	Filter Base	Filter Length
58	212203	158131	Limburg	Rukkelingen Loon-Bovelingen	TR	PT	4020–007	97.9	Gu	15.6	60.5	44.9	25.40	18.0	30.0	12.0
59	223292	159011	Limburg	Lauw - Tongeren	HS	PT	4021–001	94.2	Gu	10.5	62.3	51.8	173.00	13.0	31.5	18.5
60	227228	163274	Limburg	Lauw - Tongeren	HS	PT	4021–010	89.1	Ma	29.4	109.2	79.8	2.47	30.0	59.0	29.0
61	228767	160291	Limburg	Diets-Heur	HS	PT	4022–002	102.3	Gu	4.6	82.4	77.8	152.00	32.5	68.5	36.0
62	228792	160323	Limburg	Diets-Heur	HS	PT	4022–003	102.3	Gu	4.6	82.4	77.8	171.25	29.5	59.5	30.0
63	216994	193337	Limburg	Heusden	HS	Modflow	4027–001	51.3	Ma	363.0	620.7	257.7	2.00	363.7	400.3	36.7
64	217308	193491	Limburg	Heusden	HS	Modflow	4027–003	65	Ho/Ma	390.1	633.5	243.4	2.00	388.5	439.4	50.9
65	205877	172555	Limburg	Binderveld	TR	PT	4029–001	31.4	Ma	92.0	209.4	117.4	1.88	96.0	141.0	45.0
66	219370	176967	Limburg	Willekensmolen – Trekschuren	HS	Invers model	4030–006	61.5	Ma	135.0	289.7	154.7	2.10	136.7	183.0	46.3
67	229081	162232	Limburg	Overhaem	HS	MLU	4031–001	95.8	Ma/Gu	23.8	97.9	74.1	6.58	23.0	53.0	30.0
68	224225	171945	Limburg	Wintershoven	TR	PT	P2	46.5	Ho/Ma/Gu	39.1	203.9	164.8	16.00	50.0	99.0	49.0

Data availability

The data is included as an Appendix

References

Batelaan, O., Meyus, Y., De Smedt, F., 2007. De grondwatervoeding van Vlaanderen [The groundwater supply of Flanders]. Abstracts for Congress Water System Knowledge Study Day for Recent developments in groundwater research in Flanders, pp. 64–71.

Bauer, S., Liedl, R., Sauter, M., 2003. Modeling of karst aquifer genesis: influence of exchange flow. Water Resour. Res 39. https://doi.org/10.1029/2003WR002218.

Belgian Federal Government, 2024. Structure of the population. Struct. Popul. 2024. ⟨https://statbel.fgov.be/en/themes/population/structure-population⟩. Accessed 16 Jul.

Casillas-Trasvina, A., Rogiers, B., Beerten, K., Wouters, L., Walraevens, K., 2022. Exploring the hydrological effects of normal faults at the boundary of the Roer Valley Graben in Belgium using a catchment-scale groundwater flow model. Hydrogeol. J. 30, 133–149. https://doi.org/10.1007/s10040-021-02423-y.

Coetsiers, M., Blaser, P., Martens, K., Walraevens, K., 2009. Natural background levels and threshold values for groundwater in fluvial Pleistocene and Tertiary marine aquifers in Flanders, Belgium. Environ. Geol. 57, 1155–1168. https://doi.org/10.1007/s00254-008-1412-z.

Cooper Jr H., Jacob C.E. (1946) A Generalized Graphical Method for Evaluating Formation Constants and Summarizing Well-field History. Eos Trans AGU 27: 526–534. https://doi.org/10.1029/TR027i004p00526.

Coordinated Commission for Integrated Water Policy -CIW-, 2016. Stroomgebiedbeheerplannen voor Schelde en Maas 2016-2021. River basin management plans for Scheldt and Meuse 2016-2021. Flemish Environment Agency, Aalst, Belgium.

Dagan, G., 2002. An overview of stochastic modeling of groundwater flow and transport: From theory to applications. Eos Trans. Am. Geophys. Union 83, 621–625. https://doi.org/10.1029/2002EO000421.

Dassargues, A., Monjoie, A., 1993. Belgium. In: Downing, R.A., Price, M., Jones, G.P. (Eds.), The Hydrogeology of the Chalk of North-West Europe. Oxford University Press, pp. 153–169. https://doi.org/10.1093/oso/9780198542858.001.0001.

Databank Ondergrond Vlaanderen (2019) G3Dv3 model.

De Watergroep (1993) Verkenningsboringen in het Krijt (1993): Heverlee Abdij VB1, Heverlee Cadol VB2, Kessel-lo Vlierbeek VB3 [Exploration drilling in the Cretaceous (1993): Heverlee Abbey VB1, Heverlee Cadol VB2, and Kessel-lo Vlierbeek VB3].

De Watergroep (1978) Overijse, Kouterstraat.

De Watergroep (1988) Korbeek-Dijle Het Broek.

De Watergroep (2001) Waterwinning Overijse/Venusberg Krijt: Proefpomping op verkenningsboring 3011-005 [Water extraction Overijse/Venusberg Chalk: Test pumping on exploration well 3011-005].

De Watergroep (2004a) Hydrogeologische studie: Overijse Sana-Tombeek [Hydrogeological study: Overijse Sana-Tombeek].

De Watergroep (2004b) Hydrogeologische studie: Sint-Agatha-Rode Veeweyde [Hydrogeological study: Sint-Agatha-Rode Veeweyde].

De Watergroep (2010) Hydrogeologische studie: Grondwaterwinning in het Krijt te Heverlee Abdij [Hydrogeological study: Cretaceous groundwater extraction at Heverlee Abbey].

De Watergroep (2013) Aanleg van productieput 3010-017. Productieput in de Formatie van Hannut (Lid van Lincent) en Gulpen [Construction of production well 3010-017. Production well in the Formation of Hannut (Member of Lincent) and Gulpen].

De Watergroep (2015) Hydrogeologische studie: Grondwaterwinning in het Krijt te Overijse Nellebeek Krijt [Hydrogeological study: Cretaceous groundwater extraction at Overijse Nellebeek Cretaceous].

De Watergroep, 2016. Aanleg van productieput 3010-018. Productieput in de Formatie van Hannut (Lid van Lincent) en Gulpen [Construction of production well 3010-018. Production well in the Formation of Hannut (Member of Lincent) and Gulpen].

De Watergroep (2017a) Boren productieput 3008-063 en -064, boren peilput 3008-065 en -066 [Drilling production well 3008-063 and -064, drilling monitoring well 3008-065 and -066].

De Watergroep (2017b) Boren productieput 3012-059. Winning Sint-Agatha-Rode-Veeweyde [Drilling production well 3012-059. Extraction Sint-Agatha-Rode-Veeweyde].

De Watergroep (2017c) Hoeilaart 3023-021 en 024 [Hoeilaart 3023-021 and 024].

De Watergroep (2017d) Vilvoorde 3014-004 en 005 [Vilvoorde 3014-004 and 005].

De Watergroep (2021) Grondwaterwinning Sint-Agatha-Rode Geuzenhoek: Hydrogeologische studie van de grondwaterwinning (Krijt) [Groundwater extraction Sint-Agatha-Rode Geuzenhoek: Hydrogeological study of the Groundwater extraction (Cretaceous)].

Deckers, J., De Koninck, R., Bos, S., Broothaers, M., Dirix, K., Hambsch, L., Lagrou, D., Lanckacker, T., Matthijs, J., Rombaut, B., Van Baelen, K., Van Haren, T., 2019. Geologisch (G3Dv3) en hydrogeologisch (H3D) 3D-lagenmodel van Vlaanderen [Geological (G3Dv3) and hydrogeological (H3D) 3D layer model of Flanders]. Vlaams kenniscentrum ondergrond (VLAKO). Vlaamse Milieumaatschappij, and VITO, Mol, Belgium.

Digital Flanders Agency (2014) LiDAR Digital Elevation Model Flanders II.

Dusar, M., Lagrou, D., 2007. Lithofacies and paleogeographic distribution of the latest Cretaceous deposits exposed in the Hinnisdael underground quarries in Vechmaal (commune Heers, Belgian Limbourg). Geol. Belg. 10, 176–181.

Flemish Environment Agency (2023) Drinkwaterbalans voor Vlaanderen 2022 [Drinking water balance for Flanders – 2022]. Flemish Environment Agency.

Ghysels, G., Mustafa, S.M.T., 2021. CHalk AquifeR Management (CHARM): analysing the capacity of the Cretaceous Aquifer in Brabant, Belgium. Joint Research Programme: KWR. De Watergroep and Vrije Universiteit Brussel, Brussels, Belgium.

Gillon, M., Renard, F., Crançon, P., Aupiais, J., 2012. Kinetics of incongruent dissolution of carbonates in a Chalk aquifer using reverse flow modelling. J. Hydrol. 420 329–339. https://doi.org/10.1016/j.jhydrol.2011.12.025.

Goderniaux, P., Orban, P., Rorive, A., Brouyère, S., Dassargues, A., 2023. Study of historical groundwater level changes in two Belgian chalk aquifers in the context of climate change impacts. In: Farrell, R.P., Massei, N., Foley, A.E., Howlett, P.R., West, L.J. (Eds.), The Chalk Aquifers of Northern Europe. The Geological Society of London, pp. 203–212. https://doi.org/10.1144/SP517-2020-212.

Hantush, M.S., Jacob, C.E., 1955. Non-steady radial flow in an infinite leaky aquifer. Eos Trans. AGU 36, 95–100. https://doi.org/10.1029/TR036i001p00095.

Harbaugh, A.W., 2005. MODFLOW-2005, the US Geological Survey modular ground-water model: the ground-water flow process. US Geological Survey, Reston, USA. https://doi.org/10.3133/tm6A16.

Hartmann, A., Goldscheider, N., Wagener, T., Lange, J., Weiler, M., 2014. Karst water resources in a changing world: Review of hydrological modeling approaches. Rev. Geophys 52, 218–242. https://doi.org/10.1002/2013RG000443.

Hemker, C., 1999. Transient well flow in layered aquifer systems: the uniform well-face drawdown solution. J. Hydrol. 225, 19–44. https://doi.org/10.1016/S0022-1694(99)00093-1.

Hemker K., Post V. (2013) MLU for Windows: well flow modeling in multilayer aquifer systems. MLU User's guide.

Huysmans, M., Dassargues, A., 2009. Application of multiple-point geostatistics on modelling groundwater flow and transport in a cross-bedded aquifer. Hydrogeol. J. 17, 1901–1911. https://doi.org/10.1007/s10040-009-0495-2.

Huysmans, M., Peeters, L., Moermans, G., Dassargues, A., 2008. Relating small-scale sedimentary structures and permeability in a cross-bedded aquifer. J. Hydrol. 361, 41–51. https://doi.org/10.1016/j.jhydrol.2008.07.047.

Jacob, C.E., 1947. Drawdown test to determine effective radius of artesian well. Trans. Am. Soc. Civ. Eng. 112, 1047–1064. https://doi.org/10.1061/TACEAT.0006033.

Kordilla, J., Sauter, M., Reimann, T., Geyer, T., 2012. Simulation of saturated and unsaturated flow in karst systems at catchment scale using a double continuum approach. Hydrol. Earth Syst. Sc. 16, 3909–3923. https://doi.org/10.5194/hess-16-3909-2012.

Kovács, A., 2021. Quantitative classification of carbonate aquifers based on hydrodynamic behaviour. Hydrogeol. J. 29, 33–52. https://doi.org/10.1007/s10040-020-02285-w.
Lagrou, D., Dreesen, R., 2005. Kartering en karakterisering (sediment petrografisch en petrofysisch) van de Krijtgesteenten in Vlaanderen [Mapping and characterisation (sediment petrographic and petrophysical) of Cretaceous rocks in Flanders]. Vlaams Kennis Ondergr. (VLAKO) VITO.
Lagrou, D., Dreesen, R., 2011. Kartering en karakterisering (sediment petrografisch en petrofysisch) van de Krijtgesteenten in Vlaanderen [Mapping and characterisation (sediment petrographic and petrophysical) of Cretaceous rocks in Flanders]. Vlaams Kennis Ondergr. (VLAKO) VITO.
LeGrand R. (1968) The Brabant massif.
Liedl, R., Sauter, M., Hückinghaus, D., Clemens, T., Teutsch, G., 2003. Simulation of the development of karst aquifers using a coupled continuum pipe flow model. Water Resour. Res 39. https://doi.org/10.1029/2001WR001206.
Maréchal, J.-C., Rouillard, J., 2020. Groundwater in France: resources, use and management issues. In: Rinaudo, J.-D., Holley, C., Barnett, S., Montginoul, M. (Eds.), Sustainable Groundwater Management. A Comparative Analysis of French and Australian Policies and Implications to Other Countries. Springer, pp. 17–45. https://doi.org/10.1007/978-3-030-32766-8_2.
Matthijs, J., Lagrou, D., 2007. Diepte- en diktekaarten van de Krijtsedimenten in Vlaanderen [Depth and thickness maps of the Cretaceous sediments in Flanders]. Vito Mol. Belg.
Matthijs, J., Lagrou, D., 2010. Opbouw van een geologisch 3D lagenmodel: Lithostratigrafische indeling van de afzettingen uit het Krijt [Construction of a 3D geological layer model: lithostratigraphic classification of deposits from the Cretaceous period]. Vito Mol. Belg.
Mendizabal, I., Stuyfzand, P.J., 2009. Guidelines for interpreting hydrochemical patterns in data from public supply well fields and their value for natural background groundwater quality determination. J. Hydrol. 379, 151–163. https://doi.org/10.1016/j.jhydrol.2009.10.001.
Mustafa, S.M.T., Nossent, J., Ghysels, G., Huysmans, M., 2020. Integrated Bayesian Multi-model approach to quantify input, parameter and conceptual model structure uncertainty in groundwater modeling. Environ. Model. Softw. 126, 104654. https://doi.org/10.1016/j.envsoft.2020.104654.
National Geographic Institute (2022) Digital Terrain Model.
Nativ, R., Adar, E., Assaf, L., Nygaard, E., 2003. Characterization of the hydraulic properties of fractures in chalk. Groundwater 41, 532–543. https://doi.org/10.1111/j.1745-6584.2003.tb02387.x.
Nygaard, E., 1993. Denmark. In: Downing, R.A., Price, M., Jones, G.P. (Eds.), The Hydrogeology of the Chalk of North-West Europe. Oxford University Press, pp. 186–207. https://doi.org/10.1093/oso/9780198542858.003.0010.
Pappalardo, G., Borsi, I., Rossetto, R., Tranchina, G., Bongiovanni, M., Farina, M., Mineo, S., 2024. Unravelling the influence of heterogeneities and abstraction on groundwater flow and solute transport in a fractured carbonate aquifer, Sicily, Italy. Hydrogeol. J. 32, 1071–1083. https://doi.org/10.1007/s10040-024-02794-y.
Possemiers, M., Huysmans, M., Batelaan, O., 2014. Influence of aquifer thermal energy storage on groundwater quality: a review illustrated by seven case studies from Belgium. J. Hydrol. Reg. Stud. 2, 20–34. https://doi.org/10.1016/j.ejrh.2014.08.001.
Possemiers, M., Huysmans, M., Peeters, L., Batelaan, O., Dassargues, A., 2012. Relationship between sedimentary features and permeability at different scales in the Brussels Sands. Geol. Belg. 15, 156–164.
Rakovec, O., Samaniego, L., Hari, V., Markonis, Y., Moravec, V., Thober, S., Hanel, M., Kumar, R., 2022. The 2018–2020 multi-year drought sets a new benchmark in Europe. Earth's Future 10, 1–11. https://doi.org/10.1029/2021EF002394.
Riediger, J., Breckling, B., Nuske, R.S., Schröder, W., 2014. Will climate change increase irrigation requirements in agriculture of Central Europe? A simulation study for Northern Germany. Environ. Sci. Eur. 26, 1–13. https://doi.org/10.1186/s12302-014-0018-1.
Rogiers, B., Beerten, K., Smeekens, T., Mallants, D., Gedeon, M., Huysmans, M., Batelaan, O., Dassargues, A., 2013. Derivation of flow and transport parameters from outcropping sediments of the Neogene aquifer, Belgium. Geol. Belg. 16, 129–148.
Rogiers, B., Mallants, D., Batelaan, O., Gedeon, M., Huysmans, M., Dassargues, A., 2012. Estimation of hydraulic conductivity and its uncertainty from grain-size data using GLUE and artificial neural networks. Math. Geosci. 44, 739–763. https://doi.org/10.1007/s11004-012-9409-2.
Speijer, L., Six, S., van der Grift, B., Cirkel, D.G., Verreydt, G., Dams, J., Huysmans, M., 2024. Enhancing groundwater recharge in drinking water protection zones in Flanders (Belgium): a novel approach to assess stormwater managed aquifer recharge potential. J. Hydrol. Reg. Stud. 53, 101747. https://doi.org/10.1016/j.ejrh.2024.101747.
Theis, C.V., 1935. The relation between the lowering of the piezometric surface and the rate and duration of discharge of a well using ground-water storage. Eos Trans. AGU 16, 519–524. https://doi.org/10.1029/TR016i002p00519.
Van Camp, M., Lams, D., Walraevens, K., 2017. Hydrodynamical and hydrochemical groundwater controls on abiotic environmental gradients in a nature reserve in Flanders (Belgium). Environ. Earth Sci. 76, 1–21. https://doi.org/10.1007/s12665-017-6413-3.
Vandersteen, K., Gedeon, M., Beerten, K., 2014. A synthesis of hydraulic conductivity measurements of the subsurface in Northeastern Belgium. Geol. Belg. 17, 196–210.
Vansteenkiste, T., Dewelde, J., Cabus, P., de Jongh, I., Cauwenberghs, K., 2016. Concepts and applications of the Flanders Hydrological Model environment. EDP Sci. Lyon Fr. 04006. https://doi.org/10.1051/e3sconf/20160704006.
West, L.J., Farrell, R.P., Foley, A.E., Howlett, P.R., Massei, N., 2023. An Introduction to the chalk aquifers of Northern Europe. In: Farrell, R.P., Massei, N., Foley, A.E., Howlett, P.R., West, L.J. (Eds.), The Chalk Aquifers of Northern Europe. The Geological Society of London, pp. 1–14. https://doi.org/10.1144/SP517-2020-212.
Worthington, S.R., 2023. Examining the assumptions of the single-porosity archetype for transport in bedrock aquifers. Hydrogeol. J. 31, 87–96. https://doi.org/10.1007/s10040-022-02576-4.
Xanke, J., Goldscheider, N., Bakalowicz, M., Barberá, J.A., Broda, S., Chen, Z., Ghanmi, M., Günther, A., Hartmann, A., Jourde, H., Liesch, T., Mudarra, M., Petitta, M., Ravbar, N., Stevanović, Z., 2024. Carbonate rocks and karst water resources in the Mediterranean region. Hydrogeol. J. 32, 1397–1418. https://doi.org/10.1007/s10040-024-02810-1.
Zomlot, Z., Verbeiren, B., Huysmans, M., Batelaan, O., 2015. Spatial distribution of groundwater recharge and base flow: assessment of controlling factors. J. Hydrol. Reg. Stud. 4, 349–368. https://doi.org/10.1016/j.ejrh.2015.07.005.
Zwertvaegher, A., Finke, P., De Reu, J., Vandenbohede, A., Lebbe, L., Bats, M., De Clercq, W., De Smedt, P., Gelorini, V., Sergant, J., 2013. Reconstructing phreatic palaeogroundwater levels in a geoarchaeological context: a case study in Flanders, Belgium. Geoarchaeology 28, 170–189. https://doi.org/10.1002/gea.21435.